Opposite annular responses of the Northern and Southern Hemisphere to Indian Ocean warming

Shuanglin Li[1], Judith Perlwitz[2,3], Martin P. Hoerling[3],and Xiaoting Chen[1]

(1) Nansen-Zhu International Research Centre, Institute of Atmospheric Physics, Chinese Academy of Sciences, Beijing, China

(2) Cooperative Institute for Research in Environmental Sciences, University of Colorado, Boulder, Colorado, USA

(3) NOAA Earth System Research Laboratory, Physical Sciences Division, Boulder, Colorado, USA

Revised for J. Climate, January 2010

Corresponding author address:
Dr. Shuanglin Li, Nansen-Zhu International Research Centre, Institute of Atmospheric Physics, Chinese Academy of Sciences, Beijing 100029, China
E-mail: shuanglin.li@mail.iap.ac.cn

Abstract

Atmospheric circulation changes during boreal winter of the second half of the 20th century exhibit a trend toward the positive polarity of both the Northern Hemisphere Annular Mode (NAM) and the Southern Hemisphere Annular Mode (SAM). This has occurred in concert with other trends in the climate system, most notably a warming of the Indian Ocean. This study explores whether the tropical Indian Ocean warming played a role in forcing these annular trends. Five different atmospheric general circulation models (AGCMs) are forced with an idealized, transient warming of Indian Ocean sea surface temperature anomalies (SSTA), the results of which indicate that the warming contributed to the annular trend in the Northern Hemisphere (NH) but offset the annular trend in the Southern Hemisphere (SH). The latter result implies that the Indian Ocean warming may have partly cancelled the influence of the stratospheric ozone depletion over the southern polar area which itself forced a trend toward the positive phase of the SAM. Diagnosis of the physical mechanisms for the annular responses indicates that the direct impact of the diabatic heating induced by the Indian Ocean warming does not account for the annular response in the extratropics. Instead, interactions between the forced stationary wave anomalies and transient eddies is key for the formation of annular structures.

1. **Introduction**

The atmospheric circulation of both the Northern and Southern hemispheres (NH and SH hereafter) in the boreal winter exhibited a trend toward positive geopotential height anomalies at mid-latitudes and negative geopotential height anomalies over the polar areas during the second half of the 20th century (e.g., Thompson and Solomon 2002; Gillett and Thompson 2003 Hoerling et al. 2004). The spatial structure of these trends projects onto the positive phase of the Northern Hemisphere Annular Mode (NAM) and the Southern Hemisphere Annular Mode (SAM) (Thompson and Wallace 1998; 2000; Gong and Wang 1999). The NAM (SAM) is the leading mode of variability of NH (SH) extratropical circulation. Previous studies demonstrated that these modes account for a substantial part of the observed circulation change in both the NH and SH (Hurrell 1995; Thompson and Wallace 2001; Gillett et al. 2006), and understanding their cause is of great interest.

Concurrent with these extratropical circulation changes, significant warming trends occurred in the global tropical ocean, which were attributed to anthropogenic increases of greenhouse gases (Knutson et al. 1999; 2006; Hoerling et al. 2004). While warming trends over tropical Atlantic and west Pacific Oceans are modulated by substantial variability on decadal time scales, the tropical Indian Ocean (Fig. 1) is the epicenter for a detectable anthropogenic change because of its large monotonic sea surface temperature (SST) increase relative to its moderate decadal variability (Knutson et al. 2006). Previous atmospheric general circulation model (AGCM) and coupled air-sea model experiments reveal that the progressive tropical Indian Ocean warming has accounted for a significant fraction of the NH annular-like circulation trend (Hoerling et al. 2001; 2004; Li et al. 2006a). This was further confirmed by a recent study by Cassou (2008), which shows a close

relationship between the NAO and the Madden-Julian Oscillation (MJO) at the subseasonal timescale. In particular, when there is enhanced convection in the Indian Ocean, the NAO tends to be in the positive phase. This link is verified by the coherence between the reversed NAO trend (Overland and Wang 2005) and the weakened Indian Ocean SST trend after the mid-1990s. However, whether the warming has also contributed to the annular circulation trend in the SH is unclear.

Significant depletion of stratospheric ozone over the southern polar area during austral spring was observed in the recent decades. This ozone decrease reduces the absorption of shortwave solar radiation and cools the polar stratosphere, thus increases the meridional temperature gradient (Perlwitz et al. 2008). The accompanying dynamical response resulted in a one-month delay of the winter polar vortex breakdown in the stratosphere and a shift of the summertime SAM towards its positive phase (Thompson and Solomon 2002; Gillett and Thompson 2003; Perlwitz et al. 2008).

The co-existence of the two climate forcings each of which is attributable to human influences, ozone depletion and tropical oceanic warming, makes it difficult to separate their individual role in forming the observed southern climate trend with the short historical instrumental records at hand. There is therefore a need for investigating the sole effect of the tropical ocean warming. One AGCM study (Grassi et al. 2005) suggests that the tropical SST changes significantly contributed to the formation of the SAM trend together with the ozone depletion. Deser and Phillips (2009) illustrated however that tropical SST changes from 1950 to 1999 cause a shift of the SAM towards its negative phase. Similarly, Hu and Fu (2009) forced an AGCM with observed SSTs and reproduced the warming trend in the Antarctic stratosphere in recent decades.

Other studies suggest that tropical Pacific ocean warming (cooling) due to El Niño (La Niña) leads to a negative (positive) phase of the SAM (Zhou and Yu, 2004; L'Heureux and Thompson 2006). The goal of the present study is to compare NH and SH circulation sensitivities to progressive tropical Indian Ocean warming using experiments with AGCMs, and to understand plausible mechanisms using diagnostic models.

The paper is organized as follows. Section 2 describes the methodology employed in this study. It also introduces the five AGCMs and the linear baroclinic model (LMB) utilized. Section 3 describes the results, while discussing the circulation response in one AGCM in more detail. Section 4 explores the physical processes for the modeled annular response by diagnosing transient experiments with two AGCMs as well as with a steady state linear baroclinic model (LBM). Summary and discussions are given in the section 5.

2. **Methodology**

2.1 Sensitivity experiments

A series of idealized transient SST warming ensemble experiments were conducted using five AGCMs, the details of which are given in Table 1. Ensemble size for individual AGCMs varies from 5 to 11. For each simulation, the model is integrated over 12 years (from year 0 to 11) during which Indian Ocean SSTs are subjected to a linear rate of SST increase. More detailed information about the AGCMs and the experiments can be found in Li et al. (2008).

The progressive Indian Ocean warming is represented by forcing the ACGM with a linearly increasing SST anomaly (SSTA) within the tropical Indian Ocean basin domain as indicated in Fig. 1. The SSTA maximizes over the equatorial Indian Ocean from 5^{o}S to 5^{o}N, 40^{o}E to 110^{o}E, and

gradually decreases in amplitude to zero over 30°N and 30°S. Repeating annual cycle climatological SSTs are prescribed in the remaining ocean domain. The pattern of Indian Ocean warmth is kept fixed during the integration, whereas the amplitude increases linearly. For January of the first model year (noted as model year 0), the maximum SSTA over the equatorial areas is near zero, and then it increases with the constant rate of 0.2K per year and reaches 2.2°C at the end of the model integration (December of model year 11). Model year 0 is discarded to allow for model spin-up. The mean of the SSTA over the equatorial Indian Ocean is 0.5K for the first 5-year period (model years 1 to 5) and 1.5°C for the second 5-year period (model years 6 to 10). Thus, the SSTA difference between the second and first 5-year period has a value of 1.0 K, which is similar to the observed warming that occurred over the Indian Ocean during the second half of the 20th century (Hoerling et al. 2004; also Fig. 1).

2.2 Diagnostic experiments

A second set of experiments is carried out using two of the AGCMs (CCM3 and GFS) to diagnose physical processes leading to the formation of extratropical circulation responses. We investigate the transient atmospheric adjustment to a sudden switch-on of the idealized 1K Indian Ocean SSTA pattern. For each model, we carried out an ensemble of 60 runs with the anomalous SST forcing. Each run starts from randomly selected 1 January atmospheric initial conditions and is integrated over 45 days when the atmospheric anomalies were equilibrated. The 60-member ensemble is compared with a control ensemble of the same size forced only with climatological SST. The daily evolving differences in atmospheric states between these parallel ensemble averages are analyzed based on five day means and the statistical significance of the differences are

estimated using a Student's t-test. Such an experimental design had been used previously in Hoerling et al. (2004) using CCM3, and here we repeat that analysis using a different model.

A linear baroclinic model (LBM) is used to investigate the direct atmospheric response to a tropical forcing. The LBM is the same as used by Peng and Whitaker (1999). It is a time-dependent spectral model with a horizontal resolution of T21 and 10 equally spaced pressure levels. No topography is prescribed. The linearization is about a three-dimensional time-mean flow. The model treats the diabatic heating and the transient-eddy flux of vorticity as forcings. The basic state is calculated from the ensemble winter (DJF) or summer (JJA) mean of the 10 year detrended data in each CCM3 equilibrium experiments. Rayleigh friction and Newtonian damping have rates of $(1\ \text{day})^{-1}$ at the lowest level and $(7\ \text{days})^{-1}$ at other levels. Biharmonic horizontal diffusion with a coefficient of $2 \times 10^{16}\ \text{m}^4\text{s}^{-1}$ is applied everywhere, and Fickian thermal diffusion with a coefficient of $2 \times 10^{6}\ \text{m}^2\text{s}^{-1}$ is included to represent the heat fluxes by transient eddies. With these values for dissipation and diffusion, a steady response to a forcing is reached after about 40 days. Averages over the final 5 days of 40-day integrations are used to approximate the steady linear responses.

3. **Results of sensitivity experiments**

The nature of the annular mode responses occurring in the transient Indian Ocean warming experiments of the five AGCMs is first described. Because the changes are qualitatively similar among the five AGCMs, we present the results in detail only for the CCM3 and give a more general description for the other four models.

To illustrate the structure of the annular modes in the models, Figure 2 presents the leading Empirical Orthogonal Function (EOF) of NH and SH 500-hPa height in CCM3. The EOF analysis

is conducted for detrended time series of monthly 500-hPa heights for the NH (20^oN to 90^oN) and the SH (20^oS to 90^oS), respectively. The time series of the detrended height fields for all the 10 CCM3 runs are combined to form one time series of 1200 months.

Figure 2 shows the regression patterns of the first EOF. In the NH and SH these modes explain 25% and 34% of total variance, respectively. The spatial pattern depicts a height-anomaly seesaw between mid and high latitudes with anomalies north of 65^oN (south of 65^oS) closely related to anomalies of the opposite sign between 30^o and 50^oN (S). The spatial pattern strongly resembles the NAM (SAM) of observations for which previous papers have documented coherent vertical structures extending from the surface to the stratosphere (e.g., Thompson and Wallace 2000).

Two methods are used to illustrate the models' annular responses. One uses the temporal projection coefficient of monthly 500-hPa heights on the above leading NH/SH EOFs to represent the NAM/SAM index. The other uses a NH (SH) polar cap height index determined as area average of height anomalies from 65^oN (S) to 90^oN(S) which represents one main center of action of the NAM (SAM). That the latter is a reasonable proxy of NAM (SAM) behavior is confirmed by the strong temporal correlation of -0.79 (-0.92) between the model's 500 hPa NH (SH) polar cap height index and the NAM (SAM) index.

Figure 3 summarizes the seasonal cycle of changes in the annular mode indices and polar cap height indices, derived by computing the difference between the second and first 5-year periods of the transient simulations (see section 2.1 for detailed description). Figure 3 also shows changes

in the normalized 500 hPa North Atlantic Oscillation (NAO) index[1] which is closely related to the NAM but whose centers of action are more confined to the North Atlantic region. During the boreal cold season (December to April), the progressive Indian Ocean warming causes a significant shift of the NAM/NAO index towards its positive polarity (Fig.3a, c). This result is consistent with the previous study by Hoerling et al. (2004). During May to November, tropical Indian Ocean warming does not induce annular mode like changes as indicated by the very small response in the model's NAM index.

The SH also exhibits annular mode sensitivity to Indian Ocean warming, but interestingly having polarity opposite to the NH response. The SH response is dominated by a shift of the SAM index towards its negative phase (Fig. 3b) and, as too for the NH, exhibits greatest sensitivity during December to April (Fig.3e). During austral winter (June to August), the indices of the annular mode (polar cap height index, SAM index) do not show any significant response. Note also that for both hemispheres, the equivalent barotropic polar cap height responses (Figs. 3d, e) indicate that annular responses extend through the whole troposphere.

The regional and seasonal structures in the extratropical circulation response can be illustrated further by presenting the pattern of 200 hPa height changes for DJF and JJA (Fig. 4). Clearly, during DJF both the NH (SH) height fields show negative (positive) changes over high latitudes and positive (negative) height anomalies over mid-latitudes consistent with the NAM and SAM changes. During JJA, the NH change pattern is dominated by positive changes over most of the hemisphere with no pronounced annular structure. The SH change pattern is dominated by a

[1] We determined the 500-hPa NAO index as the different between geopotential height anomalies in a southern box (30^{o}N-50^{o}N, 80^{o}W to 20^{o}E) and a northern box (60^{o}N-80^{o}N, 80^{o}W-20^{o}W) similar to Hoerling et al. (2004)

well-organized mid-latitude wave train. We speculate that the SAM response occurs mostly in the summer season because of sensitivity to the spatial structure of the background flow and the occurrence of a single eddy-driven jet.

The above annular responses to Indian Ocean warming are further quantified by calculating the frequency of occurrence of NAM/SAM index values during the boreal winter months (DJF) for the two 5-year periods (Figure 5). For the NH, the number of months with a positive NAM index increases in the second 5-year period relative to the first 5-year period. For the SH, the situation is opposite, and the number of months with negative values increases. There is also an apparent increase in skewness of the SAM distribution as the Indian Ocean warms, with a substantial increase in extreme negative SAM states. It is unclear whether these extreme event changes are statistically significant, nor do we have a theory to understand such sensitivity. Little evidence for skewness change is seen in the NH.

In summary, the CCM3 results reveal that the SH annular mode sensitivity to tropical Indian Ocean warming is very different from its NH counterpart. First, the polarity is opposite. Second, the phasing with the seasonal cycle is also opposite with the SAM sensitivity greatest in austral summer but the NAM sensitivity greatest in boreal winter. It is plausible that model biases in simulation of the climatological seasonal cycle, and/or its sensitivity to Indian Ocean forcing could render these results unique to CCM3. However, that these findings are not an artifact of a single model is confirmed by a multi-model analysis (Fig. 6 and also Table 2), which demonstrates identical opposing behaviors of annular responses between the hemispheres. Somewhat less reproducible is the distinct seasonality of responses seen in CCM3, with more complicated monthly varying sensitivity occurring especially in the ECHAM and GFDL models.

Two additional features of the sensitivity to Indian Ocean warming are noteworthy, as they are key not only to understanding the structure of atmospheric responses but also to provide mechanisms for their proximate cause. Fig. 7a shows the DJF zonal mean zonal wind changes and Fig. 8 shows the DJF precipitation changes. It is well known that the positive annular modes coincides with strong mid-latitude westerlies (Thompson and Wallace 2000), and Figure 7a shows strengthening (weakening) in the climatological westerlies of the NH (SH). The patterns can also be interpreted as a poleward (equatorward) shift of the westerlies in the NH (SH) that is consistent with a shift of the NAM (SAM) towards positive (negative) polarity.

Precipitation changes provide a picture for the principal characteristic of the tropical sensitivity to Indian Ocean warming. Figure 8 shows a marked increase in rainfall over the warming Indian Ocean, which tends to shift meridionally with the seasonal cycle of that region's monsoonal climate and the changing position of InterTropical Convergence Zone (ITCZ). Both the spatial extent and intensity of the increased rainfall are largest in DJF, despite the fact that identical patterns of SST change occur in all seasons.

4. Results of diagnostic experiments

In this section, we investigate possible processes that may contribute to the modeled annular-like responses and their polarity. We will investigate so-called transient adjustment runs, diagnosing the development of atmospheric anomalies prior to equilibration, in order to gain insights on possible causes. The suitability of studying such additional experiments in order to understand the equilibrium results of Section 3 is supported by the resemblance of the zonal-mean zonal wind response at quasi-equilibrium (roughly day 45) to the DJF seasonal mean response in

the prior runs (compare Figs. 7a and 7b). We also further investigate the role of diabatic heating associated with the tropical rainfall sensitivity in driving the extratropical circulation response (section 4.3).

4.1 Evolution of transient response

The transient atmospheric adjustment to a tropical SSTA, for instance, as studied in Jin and Hoskins (1995), can be broadly viewed as occurring on a 2-4 week time scale before equilibration. In the first week, tropical heating anomalies develop and mature while the circulation response is mostly local and tropically confined. Linear wave dynamics and a global stationary wave response mature within the second-third week. The latter can be viewed as direct linear response to a tropical heating forcing modifying the basic state resulting in the re-organization of transient eddies, which induce anomalous transient eddy flux that further interact with the evolving large scale flow. This latter feedback process is important in determining the equilibrated solution (e.g. Held et al. 1989), whose ultimate adjustment time scale is on the order of a few weeks for steady forcing. The different phases of this adjustment can be monitored in output of experiments where the SST forcing of 1°C Indian Ocean warmth is suddenly switched-on, and the subsequent daily evolution of model states is examined. These states are based on a large 60-member ensemble so as to isolate the coherent part of the forcing-response relation (see also Hoerling et al. 2004).

For the NH (left two columns of Fig. 9), the 200 hPa responses are less than half their equilibrium amplitudes at week-2, and there is virtually no indication of annularity, especially for the NH. Around week two, the NH response consists of two wave-train-like structures, one negative-phase PNA (Pacific-North America)-like emerging from the tropical central east Pacific

and the other emerging from the tropical Indian Ocean and propagating downstream toward East Asia (see the thick dashed line in the panel for the NH in days 11-15 in Fig. 9). Such a response is in agreement with linear theory about the extratropical atmospheric responses to a tropical heating (e.g., Trenberth et al. 1998). The PNA response emerging from the central east Pacific may be associated with the Walker cell anomaly linked to the Indian Ocean forcing. This result agrees with the study by Mori and Watanabe (2008) which highlights a close relationship between the negative PNA phase and Indian Ocean convection associated with the MJO. After week-two, the responses intensify and become increasingly annular in the NH. At week-4 a positive NAO-like response is seen over the North Atlantic, which is in agreement with Cassou (2008), and a northern annular response is distinguishable. The progressive buildup process of the NAM is clearly seen from the evolution of the spatial correlation coefficients of the hemispheric responses with the NAM spatial pattern (Table 3).

For the SH (right columns, Fig. 9), from the beginning to week-two the response is weak and exhibits a zonally propagating chain along 55^{o}S. Two wave trains can be seen (see the thick dashed line in the panel for the SH of Days 11-15 in Fig. 9), one Pacific-South America (PSA)-like pattern emerging from the tropical central east Pacific and the other arched chain emerging from the tropical Indian Ocean and propagating downstream toward Australia (Wang 2005). The PSA response may share the same source with the NH PNA response. From week-2 to week-4, the responses over the southern Indian and Pacific Oceans double in strength, and also alter their spatial structure. But the strongest change is over the southern Atlantic with values switching from weak positive to significant negative anomalies, and an overall midlatitude negative height pattern emerges, whereas heights within the polar cap become predominately positive. This progressive

process of the SAM response buildup can also be seen from Table 3. For both the NH and SH, the significant difference in responses averaged from week 1-2 versus weeks 4-5 suggests that the transient feedback is critical. A similar transient adjustment can be seen in the GFS experiments indicating the robustness of the anomaly evolution (Fig. 10).

Fig. 11 displays the estimated Probability Distribution Functions (PDFs) of annular mode indices of 41-45 day mean 200 hPa heights in the transient CCM3 experiments. In the forced experiments, 70% of the ensemble members yield a positive NAM response while 55% of the members yield a negative SAM response. The NAM index has greater spread relative to the control ensemble, indicating an intensification of amplitude as well. For the SAM the index is more concentrated, suggesting that a shift to negative phase is dominant. Further calculations (not shown) reveal that the largest differences of the simulated responses from annularity locate in the region from East Siberia Uplands to Bering Sea for the northern hemisphere, and in the Southern Indian Ocean off the Antarctica for the southern hemisphere.

4.2 Role of Transient momentum forcing

As indicated previously, the atmospheric responses have attained quasi-equilibrium with the SSTA forcing by 45 days, in so far as the zonal mean zonal wind anomalies at day 45 are very similar to the response in the equilibrium experiments (Fig. 7a). Now, we diagnose the role of transient eddy feedback in forming the annular responses using budget balance calculations. Dynamically, the annular mode is a transient phenomenon with a time scale of about 10 days (Luo et al. 2007). The importance of transient eddies can be further elaborated by budget diagnostics of

zonal mean zonal wind. The equation for the zonal mean zonal wind can be written as follows (Seager et al. 2003):

$$\frac{\partial <\bar{u}>}{\partial t} = -\left(\frac{<\bar{v}>}{a}\frac{\partial <\bar{u}>}{\partial \phi} + <\bar{\omega}>\frac{\partial <\bar{u}>}{\partial p}\right) + \left(f + \frac{<\bar{u}>\sin\phi}{a\cos\phi}\right)<\bar{v}>$$
$$-\frac{1}{a\cos^2\phi}\frac{\partial}{\partial \phi}\left(<u^*v^*>\cos^2\phi\right) - \frac{\partial}{\partial p}<\bar{u}^*\bar{\omega}^*>$$
$$-\frac{1}{a\cos^2\phi}\frac{\partial}{\partial \phi}\left(<\overline{u'v'}>\cos^2\phi\right) - \frac{\partial}{\partial p}<\overline{u'\omega'}> \qquad (1)$$
$$-\overline{D<u>}.$$

Here, the zonal-mean variation are divided into contributions from the zonal-mean circulation denoted as brackets, stationary waves denoted as asterisk, and transient eddies denoted as primes. The variable *u* is the zonal wind, *v* the meridional wind, *a* is the radius of the earth, ϕ is latitude, p is pressure, f is the Corislis parameter, $D<u>$ is a damping, and upper bar denotes the time mean. The first term on the right side is the advection of the zonal mean wind by the mean meridional circulation, the second term is the Coriolis torque, the third and fourth terms are the forcing by the stationary waves through inducing momentum flux convergence, and the fifth and sixth terms are the forcing by the transient eddies through inducing momentum flux convergence.

We calculate the zonal mean momentum balance for the quasi-equilibrium period of the CCM3 transient responses from day 31 to day 45. The stationary wave fluxes are calculated using 9-day running means, whereas the transient eddies are computed from the daily original value minus the 9-day running mean. The balance in the extratropics is described by a tendency of the stationary wave and transient eddy terms to induce a tendency for westerly acceleration (deceleration) near ~60°N (~60°S) that balances the Coriolis torque term (not shown). A similar

role of these terms in maintaining the ENSO-associated zonal-mean zonal wind is seen in previous studies (Seager et al. 2003; L'Heureux and Thompson 2006).

In so far as the Coriolis torque can be interpreted as a response to the stationary and transient momentum fluxes, further diagnosis of time evolving transient eddy and stationary eddy fluxes is desirable. Figure 12 displays the daily evolution of 300-hPa stationary zonal-mean zonal wind anomaly $[\bar{u}]$, anomalous stationary wave momentum forcing and synoptic transient momentum forcing. From Fig. 12a, prior to day 10 $[\bar{u}]$ is weak, especially over the extratropics, consistent with the fact that transient feedback is not involved at this stage of adjustment. From day 5 to day 15, positive $[\bar{u}]$ anomalies begin to develop in the SH subtropics, and become larger (Fig. 12a). At the same time, negative anomalies develop between 30°S and 50°S. These anomalies reach -0.5 m/s starting day 20 and increase up to about 1m/s by the end of the 45 day period while the region of negative anomalies shifts southward. These features are consistent with a southward shift of the jet. The development in the NH is characterized by an expansion of positive anomalies towards the Equator reaching amplitudes of 3 m/s at 5°N. Together with the equatorial positive wind anomaly a decrease of westerlies winds around 30°N (up to -2.5m/s) and an increase near 60°N (up to 3.5m/s) can be found. The fact that the positive zonal-mean zonal wind anomaly extends over a wider domain in the SH tropics than in the NH is related to the location of the climatological heating during this season. The diabatic heating anomaly as seen from the rainfall responses (Fig. 8a) shifts toward the south with a maximum around 10°S.

Figs. 12b and c illustrate the relative contributions of momentum flux convergence induced by stationary and transient eddies. For the NH, momentum flux convergence induced by transient eddy is evidently greater than that induced by stationary waves. Furthermore, the evolution of –

d[u'v']/dy bears more resemblances to the zonal-mean zonal wind than *–d[u*v*]/dy*, suggesting that the synoptic eddies are more important in inducing the northern annular response. For the SH, however, the two terms are more close to each other in magnitude, suggesting they jointly contribute to the formation of the negative-phase SAM trend. This is particularly clear after day 35. Thus, the relative role of stationary waves and synoptic scale eddies in inducing the annular response is different for the two hemispheres. This difference was also found in Seager et al. (2003) where the momentum budget of hemispherically symmetric zonal-mean zonal wind anomalies due to El Niño was studied. Nonetheless, the present analysis suggests that the atmospheric direct response to the tropical Indian Ocean heating is not annular. An annular response cannot be induced without transient eddy feedback.

4.3 Role of diabatic heating

The sensitivity of the annular responses to the direct tropical heating is illustrated by utilizing LBM experiments (e.g. Peng et al. 2003; Li et al. 2006b, 2007). An idealized heating is given, as shown in Fig. 13. It is largely based on the anomalous rainfall induced by the Indian Ocean SSTA (not shown), which is similar to that in Fig. 8a.

Figures 14a and b display the LBM response to the idealized heating under the DJF basic state. The NH response consist of two wave-train-like circulation anomalies, one PNA-like pattern emerging from the tropical central Pacific and the other directly emerging from the tropical Indian Ocean and propagating downstream. These wave-train like responses are not only similar to the transient responses through day 11-15 (Figs. 9 and 10), but also correspond to linear theory studies (Trenberth et al. 1998).

For the SH the LBM response is somewhat complicated, but two kinds of wave train are still discernable: an arched Rossby wave train emerging from the southern tropical Indian Ocean propagating downstream eastward to South Indian Ocean and reaching Australia; and a second wave train evolving from the central-eastern Pacific and propagating downstream eastward to South America, reminiscent of the PSA-like pattern (Wang 2005).

These responses can be explained by the linear Rossby waves excited by the tropical heating. The PNA and PSA responses may be associated with the wave source over the central-east Pacific linked to the Walker cell. That the tropical Indian Ocean triggers anomalous wave activity to influence the SH extratropics is also observed in previous studies (e.g., Quintanar and Mechoso 1995). The LBM responses in the SH are overall similar to the 5-day mean through day 16-20 in the transient runs (Fig. 9 and Fig. 10). These results support the point that the atmospheric linear response to tropical Indian Ocean forcing is not annular. High frequency transience, however, cannot fully explain the formation of the annular response from the PNA- and PSA-like pattern, since it is most typical that low-frequency eddies excite higher frequency transient eddies in a manner which reinforces the low-frequency eddies. One possible mechanism is that the Indian Ocean convection changes the refractive index for propagating waves, as discussed by Seager et al. (2003). Nonetheless, annularity does not emerge without feedback from transient eddies, which has been seen from Fig. 12 albeit discussed previously (eg. Li et al. 2006b, 2007).

The same LBM experiments is also performed under a JJA basic state with the same idealized heating except for the maximum location shift to the Bay of Bengal with intriguing results. For the NH (Fig. 14c) the JJA response is considerably weak. For the SH (Fig. 14d), the response is evidently much stronger, and its magnitude is twice or three times bigger than during DJF. This

suggests that the atmospheric direct response in the NH to a tropical Indian Ocean heating is more seasonally dependent, in agreement with the stronger seasonality of the NH response revealed in the trend experiments (e.g. Fig. 6).

5. Summary and discussion

During the second half of the 20th century, significant tropical Indian Ocean warming occurred along with a shift of SAM and NAM indices towards their positive phase. We investigated the influence of the tropical Indian Ocean warming on extratropical circulation by carrying out sensitivity studies with 5 AGCMs. The results of this study reveal that

(1) Indian Ocean warming induces an annular-like atmospheric circulation response in both hemispheres, but of opposite polarity- positive in the NH and negative in the SH.

(2) The annular responses maximize in different seasons in the hemispheres- boreal winter in the NH, and austral summer in the SH.

The simulated NH responses to Indian Ocean warming are in agreement with both the observed NAM trends and the results of previously published AGCM studies (e.g., Hoerling et al. 2001; 2004). This suggests that the Indian Ocean warming may have materially contributed to the observed NH trend. However, the simulated responses are opposite to the observed SAM trend. In so far as this was a robust sensitivity in all AGCMs, the results suggest that other forcings are dominating the observed SH trend. Stratospheric ozone depletion as described in section 1 has been previously shown to be a key factor. Our result suggests, therefore, that the impact of stratospheric ozone depletion on the SH tropospheric circulation during DJF is partly offset by the impact of

Indian Ocean Warming, and that a stronger than observed SAM trend towards its positive phase would have resulted in the absence of Indian Ocean warming.

The SAM results of the present study are in agreement with a recent study by Deser and Phillips (2009) on the relative contribution of observed circulation changes to both direct radiative forcings and to sea surface temperatures to circulation changes from 1950 to 1999. For DJF, they showed that changes in the direct atmospheric forcing (including well mixed greenhouse gases and ozone changes) cause a shift towards positive SAM index polarity, while SST changes (mainly of tropical origin) cause a shift towards its negative phase.

During the 1951-1999 period, tropical SST changes were not only characterized by Indian Ocean warming, but also by a general warming in the tropical Eastern Pacific (e.g. Fig. 9f in Deser and Philips, 2009). Thus, changes in the tropical Indian Ocean cannot be considered in isolation from changes in the tropical Pacific. On the interannual time scale, there is a significant negative correlation between the ENSO index (measured by the cold-tongue index) and the summertime SAM index (L'Heureux and Thompson, 2006, Zhou and Yu 2004). However, indices of the NAM and ENSO are not significantly correlated during any season (L'Heureux and Thompson 2006). Deser and Philips (2009) determined that the tropical warming causes positive trends in SAM index and Northern Atlantic Oscillation (NAO). The study by L'Heureux and Thompson (2006) and our study provide additional insight into the results by Deser and Philip (2009) by suggesting that warming in both tropical Indian Ocean and tropical Pacific contributed to a negative SAM trend, while Indian Ocean warming is the main tropical SST cause for the positive NAO trend. Whether possible nonlinear interaction between SST changes in the tropical Pacific and the Indian Ocean and recent changes in the trend behavior of tropical SST (cooling in tropical Pacific, leveling off of

tropical Indian Ocean warming) plays a role in the near-neutral or negative phase behavior of the NAM since the mid-1990s (e.g. Overland and Wang 2005) requires further investigation.

Our findings raise two additional questions: (1) Why do the two hemispheres yield opposite polarity annular responses to identical SST forcing which is equatorially centered and axially symmetric? (2) Why do the two hemisphere's responses maximize in opposite phases of their annual cycles? The transient adjustment experiments with two AGCMs together with the idealized heating experiments with an LBM indicate that these two questions are closely related and that more studies are necessary to answer them completely. First of all, the transient adjustment experiments indicate that the annular response was initiated by a thermally driven wave-like response followed by mid-latitude transient eddy feedback with the mean flow. A lack of a NH summer impact on the extratropical circulation can be attributed to the lack of any significant wave train-like response (Fig. 13c) and the fact, that NH stationary and transient eddy activity during that season is weak. We note that in the SH, transient eddy activity has no pronounced seasonal cycle. The spin-up experiments suggest that the differences in the polarity of the NH and SH responses result from the differences between the NH and SH climatological basic states of zonal mean zonal wind. However, further analysis and additional experiments have to be carried out for an in-depth investigation about the interhemispheric difference of climatological basic flow, transience eddy activity and their feedbacks, as well as sensitivity to the strength and location of the tropical heating anomalies.

The results of the present study have implications for the attribution of extratropical circulation changes, the role of SST changes, and the need for the investigation of the sensitivity to SST changes in individual ocean basins. An open question is how a further warming of Indian

Ocean SST combined with a possible recovery of the Antarctic ozone hole (e.g. Perlwitz et al. 2008) will reshape SH circulation changes during the next decades.

Finally, there are several limitations in this study linked especially to the idealized nature of our experiments. The prescribed rate of Indian Ocean warming is, for instance, much swifter than observed. To what extent this will influence the atmospheric trend behavior toward the annular structure is unclear. The present study may also miss possible impacts of stratospheric climate change and its impact on the extratropical troposphere. For example, none of the models analyzed included a proper simulation of stratospheric dynamics. Scaife et al. (2005) argued that realistic changes in the NAO can only be simulated when including realistic changes in the stratospheric circulation. A recent study by Lin et al. (2009) showed that increased wave forcing of stratospheric circulation in boreal spring caused a warming of the polar lower stratosphere due to an increase of the Brewer-Dobson circulation and has partly offset the cooling the stratosphere by ozone depletion. The implications on tropospheric climate change have not been studied to date.

Acknowledgements. The authors thank anonymous reviewers for constructive suggestions, which led to a significant improvement of the manuscript, acknowledge Dr. Walter Robinson for helpful discussions and Dr. Tore Furevik for commenting on an early version of the manuscript. The experiments with the GFS, the CCM3, CAM3, and the ECHAM5 models were carried out by Xiaowei Quan, Gary Bates, Adam Phillips, and Kaiming Hu, respectively. This study was jointly supported by the Innovation Key Program (Grant KZCX2-YW-BR-14) of the Chinese Academy of Sciences, the National Basic Research Program (Grant 2010CB428602) and the National Natural Science Foundation of China (Grant 40775053). The contribution of JP was supported by the

NOAA climate program office.

REFERENCES

Cassou, C., 2008: Intraseasonal interaction between the Madden-Julian Oscillation and the North Atlantic Oscillation. *Nature*, **455**, 523–527, doi:10.1038/nature07286

Collins, W. D., and Coauthors, 2006: The Community Climate System Model version 3 (CCSM3). *J. Climate*, **19**(11), 2122–2143.

Deser, C., and A. S. Phillips, 2009: Atmospheric circulation trends, 1950-2000: the relative roles of sea surface temperature forcing and direct atmospheric radiative forcing. *J. Climate*, **22**, 396-413

Gillett, N., and D. W. J. Thompson, 2003: Simulation of recent Southern Hemisphere climate change. *Science*, **302**, 273–275.

Gillett, N. P., T. D. Kell, and P. D. Jones, 2006: Regional climate impacts of the Southern Annular Mode. *Geophys. Res. Lett*., **33**, L23704, doi:10.1029/2006GL027721.

Gong, D., and S. Wang, 1999: Definition of Antarctic Oscillation index. *Geophys. Rea. Lett*., **26**, 459-462.

Grassi B., G. Redaelli, and G. Visconti, 2005: Simulation of polar Antarctic trends: Influence of tropical SST. *Geophys. Res. Lett*., **32**, L23806, doi:10.1029/2005GL023804.

Hoerling, M. P., J. W. Hurrell, and T. Xu, 2001: Tropical origins for recent North Atlantic climate change. *Science*, **292**, 90–92.

Hoerling, M. P., J. W. Hurrell, T. Xu, G. T. Bates, and A. S. Phillips, 2004: Twentieth century North Atlantic climate change. Part II: Understanding the effect of Indian Ocean warming. *Clim. Dyn*., **23**, 391-405.

Hu, Y., and Q. Fu, 2009: Antarctic stratospheric warming since 1979. *Atmos. Chem. Phys*., **9**, 4329–4340.

Hurrell, J, W., 1995: Decadal trends in the North Atlantic Oscillation: Regional temperatures and precipitation. *Science*, **269**, 676-679.

IPCC, 2007: Climate Change 2007: The Physical Science Basis. Contribution of Working Group I to the Fourth Assessment Report of the Intergovermental Panel on Climate Change. Solomon, S, D. Qin, M. Manning, et al., Eds, Cambridge University Press, Cambridge, United Kingdom and New York, NY, USA, 996.

Jin, F., and B. J. Hoskins, 1995: The direct response to tropical heating in a baroclinic atmosphere. *J. Atmos. Sci*., **52**, 307-319.

Kanamitsu, M., 1989: Description of the NMC global data assimilation and forecast system. *Wea. and Forecasting*, **4**, 335-342.

Kanamitsu, M., J. C. Alpert, K. A. Campana, P. M. Caplan, D. G. Deaven, M. Iredell, B. Katz, H.-L. Pan, J. Sela, and G. H. White, 1991: Recent changes implemented into the global forecast system at NMC. *Wea. and Forecasting*, **6**, 425-435.

Kiehl, J. T., and co-authors, 1998: The National Center for Atmospheric Research Community Climate Model: CCM3. *J. Climate,* **11,** 1131–1149.

Knutson T. R., T. L. Delworth, K. W. Dixon, and R. J. Stouffer, 1999: Model assessment of regional surface temperature trends (1949–1997). *J. Geophys. Res*., **104**, 30981–30996

Knutson, T. R., T. L. Delworth, K. W. Dixon, I. M. Held, J. Lu, V. Ramaswamy, M. D. Schwarzkopf, G. Stenchikov, and R. J. Stouffer, 2006: Assessment of twentieth-century regional surface temperature trends using the GFDL CM2 coupled models. *J. Climate*, **19**, 1624–1651.

L'Heureux, M. L., and D. W. J. Thompson, 2006: Observed relationships between the El Niño-Southern Oscillation and the extratropical zonal-mean circulation. *J. Climate,* **19**, 276-287.

Li, S., M. P. Hoerling, and S. Peng, 2006a: Coupled ocean-atmosphere response to Indian Ocean warmth. *Geophys. Res. Lett.*, **33,** 7 L07713, doi:10.1029/2005GL025558.

Li, S**.,** M. P. Hoerling, S. Peng, and K. M. Weickmann, 2006b: The annular response to tropical Pacific SST forcing. *J. Climate,* **19**(9), 1802–1819.

Li, S., W. A. Robinson, M. P. Hoerling, and K. M. Weickmann, 2007: Dynamics of the extratropical response to a tropical Atlantic SST anomaly. *J. Climate*, **20**(3), 560-574.

Li, S., J. Lu, G. Huang, and K. Hu, 2008: Tropical Indian Ocean basin warming and East Asian summer monsoon: a multiple AGCM study. *J. Climate*, **21**(22), 6080-6088.

Lin, P., Q. Fu, S. Solomon, and J. M. Wallace, 2009: Temperature Trend Patterns in Southern Hemisphere High Latitudes: Novel Indicators of Stratospheric Change. *J. Climate*, **22**, 6325–6341.

Luo, D., A. R. Lupo, and H. Wan, 2007: Dynamics of eddy-driven low-frequency dipole modes. Part I: a simple model of North Atlantic Oscillations. *J. Atmos. Sci.,* 64(1), 3–28.

Mori, M., and M. Watanabe, 2008: Growth and triggering mechanisms of the PNA: A MJO-PNA coherence. *J. Meteo. Soc. Japan*, **86** (1), 213-236.

Overland, J. E., and M. Wang, 2005: The Arctic climate paradox: the recent decrease of the Arctic Oscillation. *Geophys. Res. Lett.,* **32**(6), L06701, doi: 10.1029/2004GL021752.

Peng, S., and J. S. Whitaker, 1999: Mechanism determining the atmospheric response to midlatitude SST anomalies. *J. Climate*, **12**, 1393-1408.

Peng, S., W. A. Robinson, and S. Li, 2003: Mechanisms for the NAO responses to the North Atlantic SST tripole. *J. Climate,* **16,** 12 1987–2004.

Perlwitz, J., S. Pawson, R. L. Fogt, J. E. Nielsen, and W. D. Neff, 2008: Impact of stratospheric ozone hole recovery on Antarctic climate. *Geophys. Res. Lett.,* **35**, L08714, doi:10.1029/2008GL033317.

Quintanar, A. I., and C. R. Mechoso, 1995: Quasi-stationary waves in the southern hemisphere. Part I: observational data. *J. Climate*, **8**, 2659-2672.

Roeckner, E., and Coauthors, 2003: Atmospheric general circulation model ECHAM5. Part I: Model description. Max Planck Institute for Meteorology Rep. 349, 140 pp. [Available from Max-Planck-Institut fűr Meteorologie, Bundesstr. 55, D-20146, Hamburg, Germany.]

Scaife, A. A., J. R. Knight, G. K. Vallis, and C. K. Folland, 2005: A stratospheric influence on the winter NAO and North Atlantic surface climate. *Geophys. Res. Lett.*, **32**, L18715, doi:10.1029/2005GL023226.

Sardeshmukh, P. D., and B. J. Hoskins, 1988: The generation of global rotational flow by steady, idealized tropical divergence. *J. Atmos. Sci.*, **45**, 1228-1251.

Seager, R., N. Harnik, and Y. Kushnir, W. Robinson, and J. Miller, 2003: Mechanisms of hemispherically symmetric climate variability. *J. Climate*, **16**, 2960-2978.

The GFDL Global Atmospheric Model Development Team, 2004: The new GFDL global atmosphere and land model AM2/LM2: Evaluation with prescribed SST simulations. *J Climate*, **17,** 24 4641–4673.

Thompson, D. W. J., and J. M. Wallace, 2000: Annular Modes in the extratropical circulation. Part I: Month-to-month variability. *J. Climate*, **13**, 1000-1016.

Thompson, D. W. J., and J. M. Wallace, 2001: Regional climate impacts of the northern hemisphere annular mode. *Science*, **293**, 85–89.

Thompson, D. W. J., and J. M. Wallace, 1998: The Arctic Oscillation signature in the wintertime geopotential height and temperature fields. *Geophy. Res. Lett.,* 25(9), 1297-1300.

Thompson, D. W. J., and S. Solomon, 2002: Interpretation of recent southern hemisphere climate change. *Science,* **296**, 895.

Ting, M., and P. D. Sardeshmukh, 1993: Factors determining the extratropical responses to equatorial diabatic heating anomalies. *J. Atmos. Sci.*, **50**, 907-918.

Ting, M., and L. Yu, 1998: Steady response to tropical heating in wavy linear and nonlinear baroclinic models. *J. Atmos. Sci.*, **55**, 3565-3582.

Trenberth, K. E., G. W. Branstator, D. Karoly, A. Kumar, N.-C. Lau, and C. Popelewski, 1998: Progress during TOGA in understanding and modeling global teleconnections associated with tropical sea surface temperatures. *J. Geophys. Res*., **103**, 14 291- 14 324.

Wang, H., 2005: the circum-Pacific teleconnection pattern in meridional wind in the high troposphere. *Adv. Atmos. Sci*., **22**(3), 463–466.

Yang, E.-S., D. M. Cunnold, R. J. Salawitch, M. P. McCormick, J. Russell III, J. M. Zawodny, S. Oltmans, and M. J. Newchurch, 2006: Attribution of recovery in lower-stratospheric ozone. *J. Geophys. Res.*, 111, D17309, doi:10.1029/2005JD006371.

Zhou, T., and R. Yu, 2004: Sea-surface temperature induced variability of the Southern Annular Mode in an atmospheric general circulation model. *Geophys. Res. Lett*., 31, L24206, doi:10.1029 /2004GL021473.

Table 1: Models used for the trend simulations and ensemble size.

Model	Reference	Ensemble Size
NCAR CCM3[a]	Kiehl et al. 1998	10
NCAR CAM3[b]	Collins et al. 1998	5
NCEP GFS[c]	Kanamitsu et al. 1989; 1991	11
GFDL AM2.0[d]	The GFDL Global Atmospheric Model Development Team, (2004)	10
MPI ECHAM5[e]	Roeckner et al. 2003	9

[a]National Center for Atmospheric Sciences , Climate Community Model Version 3

[b] National Center for Atmospheric Sciences , Community Atmosphere Model Version 3

[c]National Centers for Environment Prediction, Global Forecast System

[d]Geophysical Fluid Dynamics Laboratory, Atmospheric Model Version 2.0

[e]Max Planck Institute for Meteorology, Atmospheric Model Version 5.0

Table 2 Dec-Apr mean 500-hPa NAM/SAM index changes.

	CCM3	**GFS**	**CAM3**	**AM2**	**ECHAM5**
NAM	1.11	1.10	0.65	0.34	0.27
SAM	-0.76	-0.85	-0.61	-0.26	-0.15

Table 3 The evolution of the spatial correlations of 200-hPa height responses with the NAM and SAM (EOF1 in Fig. 2) in the CCM3 diagnostic transient runs.

Days	1-5	6-10	11-15	16-20	21-25	26-30	31-35	41-45
NH	0.18	0.32	0.46	0.64	0.66	0.81	0.78	0.83
SH	0.21	0.01	-0.05	0.11	0.08	-0.04	-0.10	-0.29

Figure Captions

Fig. 1 Comparison of the SSTA used to force the AGCMs with the observed SST in the Indian Ocean. (a) and (b) are the amplitude and spatial pattern of the time-evolving SSTA used in the AGCM experiments. The amplitude is the maximum value along the equator, and the pattern is for December of year 10. Unit: K. (c) and (d) are the evolution of the observed SST averaged over (40°E-110°E, 15°S-15°N) (unit: °C) and the spatial pattern of linear trend (unit: K per 50 years) through 1950 to 1999. The dotted line represents the linear fit. The HadISST dataset is used.

Fig. 2 Regression patterns of 500-hPa heights of the leading EOF in 10 CCM3 runs. a) NH, b) SH. Unit: gpm. Shading indicates the values less than –10.

Fig. 3 Seasonal mean trend responses of the NAM/SAM index (a, b), trend response of the NAO index (c), and northern and southern polar cap mean height response (e, f) in the CCM3 experiments. The response is determined as the difference between the means of model years 6 to 10 and 1 to 5. Unit: gpm. Shading indicates statistical significance at the 95% level.

Fig. 4 200-hPa height response for the NH (left panels) and the SH (right panels) in the CCM3 experiments. (a, b) DJF, and (c, d) JJA. Unit: gpm. Shading indicates statistical significance at the 95% level.

Fig. 5 Frequency of occurrence of the NAM (a) and SAM (b) index for the first (shaded bars) and second (white bars) five-year periods in the CCM3 experiments. Results are shown for DJF months.

Fig. 6 As Figs. 3d and e, but the response in the GFS, the CAM3, the AM2, and the ECHAM5.

Fig. 7 DJF zonal-mean zonal wind response in the CCM3 equilibrium experiments (upper panel) and the averaged response through day 31-45 in the CCM3 transient runs (lower panels). Unit: m s^{-1}. Shading in (a) indicates significant at the level of 95%.

Fig. 8 Precipitation response in the CCM3 experiments. a) DJF, b) JJA. Unit: mm day^{-1}.

Fig. 9 The evolution of 200-hPa height responses in the CCM3 transient runs. Shading indicates significant at the level of 95%. Unit: gpm. The thick solid lines indicate propagation of wave trains.

Fig. 10 As Fig. 9, but for the GFS transient experiments.

Fig. 11 Estimated Probability Distribution Functions (PDFs) of the normalized 200 hPa (a) NAM and (b) SAM indices determined from 41 to 45 day mean response in the CCM3 transient runs. The solid line is for control ensemble, and the dashed line is for the Indian Ocean forced ensemble.

Fig. 12 The evolution of (a) the 300-hPa zonal-means zonal wind [u], (b) anomalous stationary wave momentum flux convergence ($-d\,[u^*v^*]/dy$), and (c) anomalous transient eddy momentum flux convergence ($-d[u'v']/dy$). Shading in (a) indicates statistical significance at the 95% level. Unit: ms^{-1} in (a), and ms^{-2} in (b, c).

Fig. 13 The in-depth mean (a) and the vertical profile of the maximum center (b) of an idealized diabatic heating centering at (70^oE, 10^oS). Unit: K day^{-1}.

Fig. 14 LBM 200-hPa geopotential height responses to the idealized diabatic heating displayed in Fig. 13. (a, b) for the NH and the SH under the winter (DJF) basic state with the maximum heating at (70^oE, 10^oS), (c, d) as (a, b), but for the summer (JJA) basic state with the maximum heating at (90^oE, 10^oN). Unit: gpm. Shading indicates values greater than 10 gpm

or less than –10 gpm in (a, d), and greater than 5 gpm or less than –5 gpm in (b, c). The thick solid lines indicate propagation of wave trains.

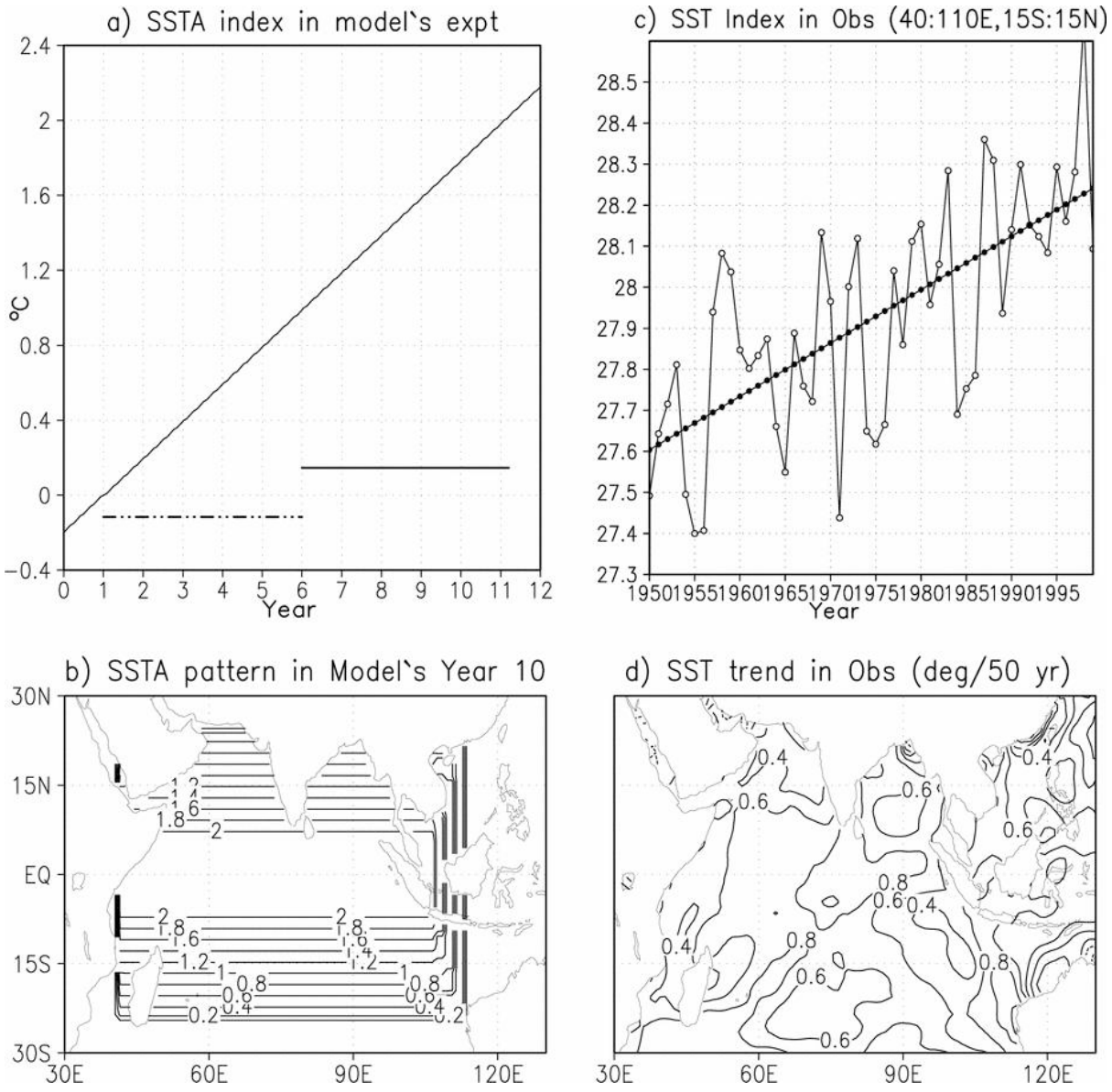

Fig. 1 Comparison of the SSTA used to force the AGCMs with the observed SST in the Indian Ocean. (a) and (b) are the amplitude and spatial pattern of the time-evolving SSTA used in the AGCM experiments. The amplitude is the maximum value along the equator, and the pattern is for December of year 10. Unit: K. (c) and (d) are the evolution of the observed SST averaged over (40^{o}E-110^{o}E, 15^{o}S-15^{o}N) (unit: ^{o}C) and the spatial pattern of linear trend (unit: K per 50 years) through 1950 to 1999. The dotted line represents the linear fit. The HadISST dataset is used.

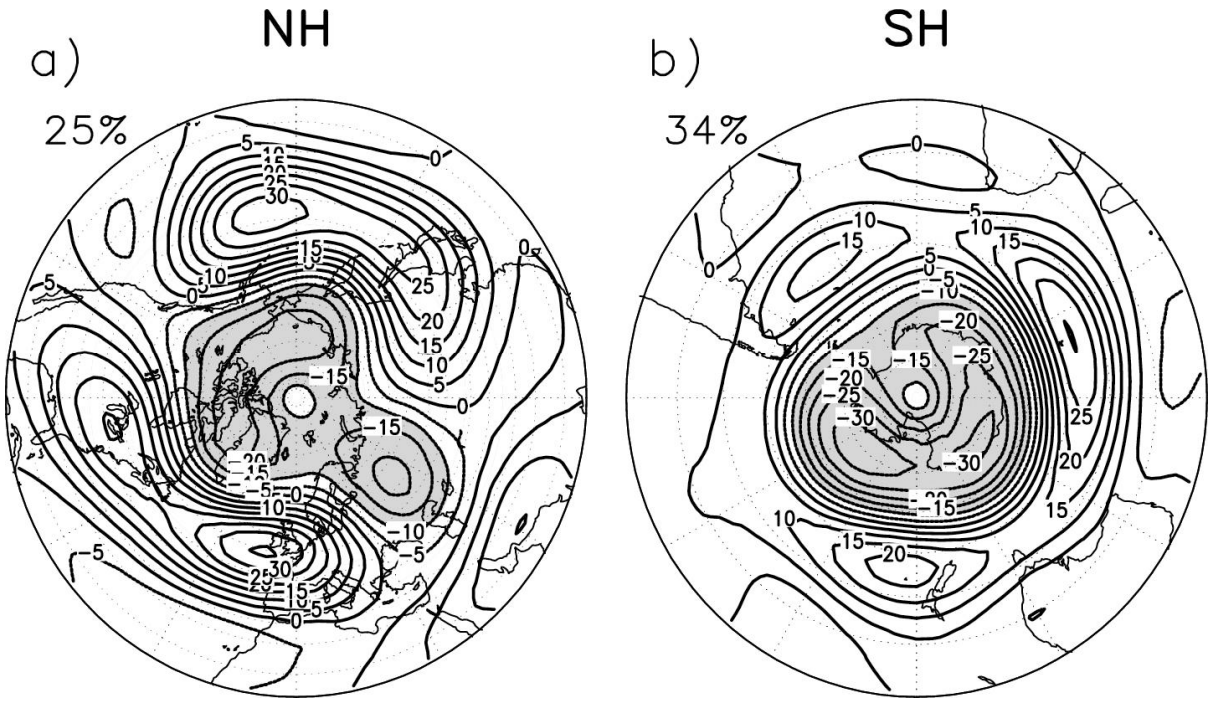

Fig. 2 Regression patterns of 500-hPa heights of the leading EOF in 10 CCM3 runs. a) NH, b) SH. Unit: gpm. Shading indicates the values less than –10.

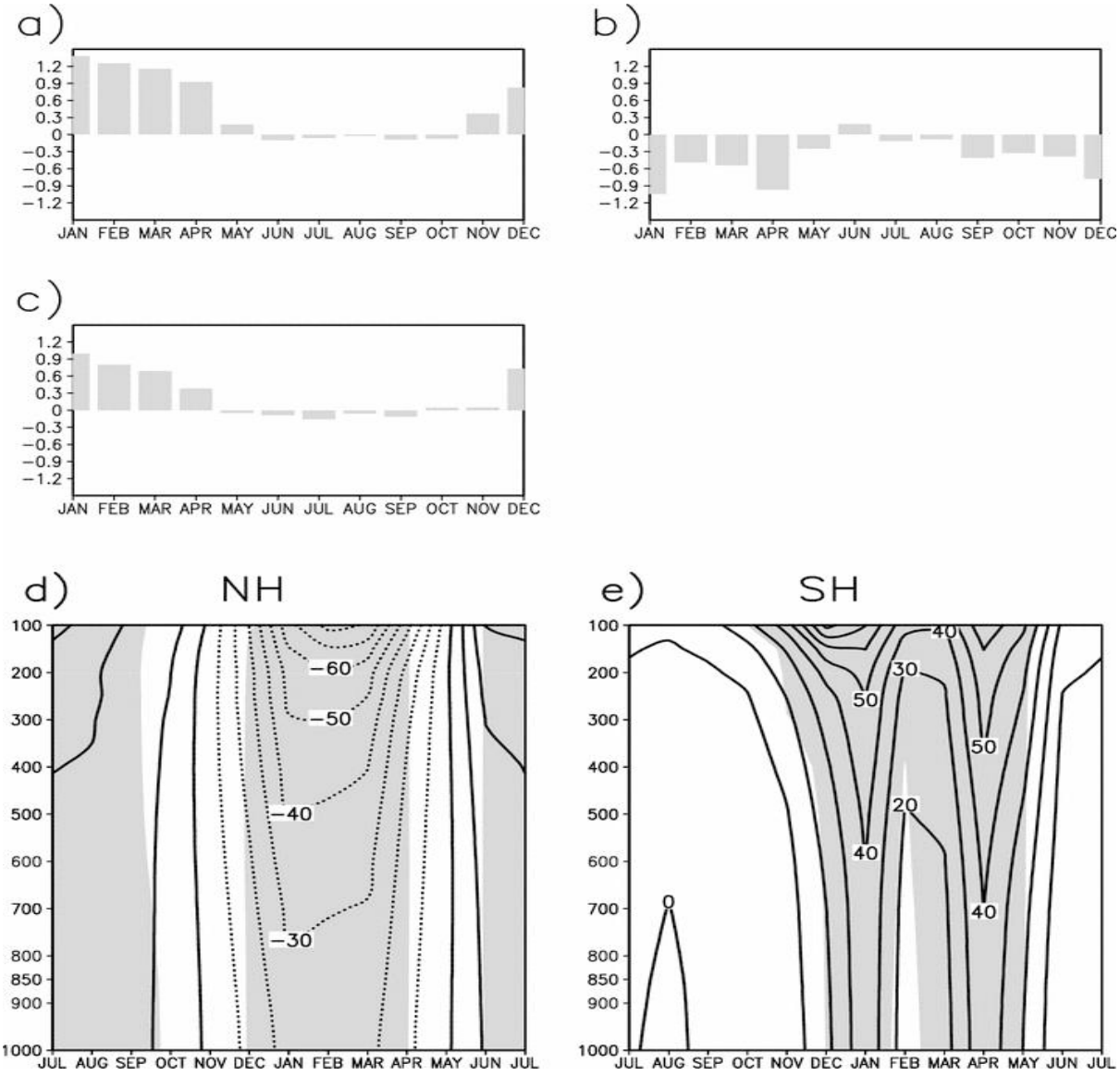

Fig. 3 Seasonal mean trend responses of the NAM/SAM index (a, b), trend response of the NAO index (c), and northern and southern polar cap mean height response (e, f) in the CCM3 experiments. The response is determined as the difference between the means of model years 6 to 10 and 1 to 5. Unit: gpm. Shading indicates statistical significance at the 95% level.

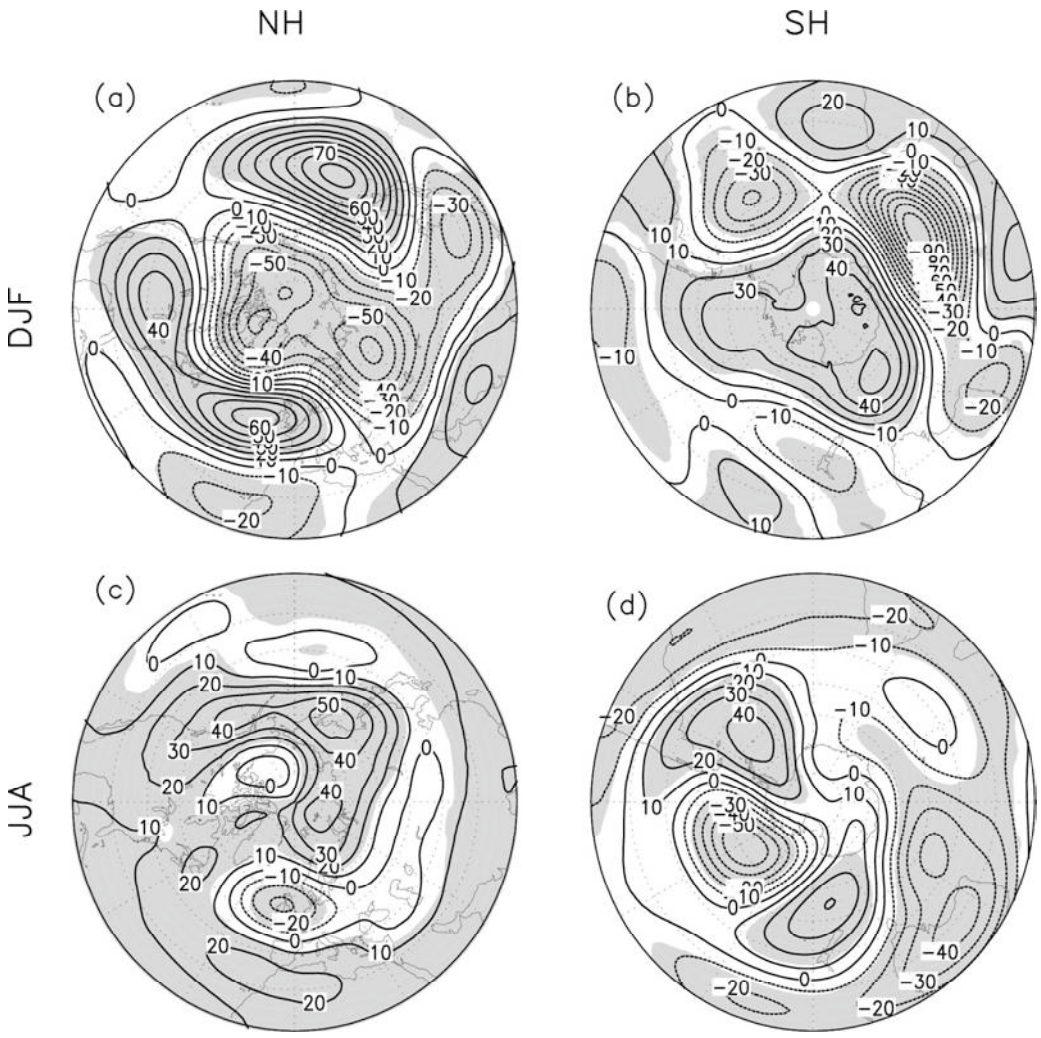

Fig. 4 200-hPa height response for the NH (left panels) and the SH (right panels) in the CCM3 experiments. (a, b) DJF, and (c, d) JJA. Unit: gpm. Shading indicates statistical significance at the 95% level.

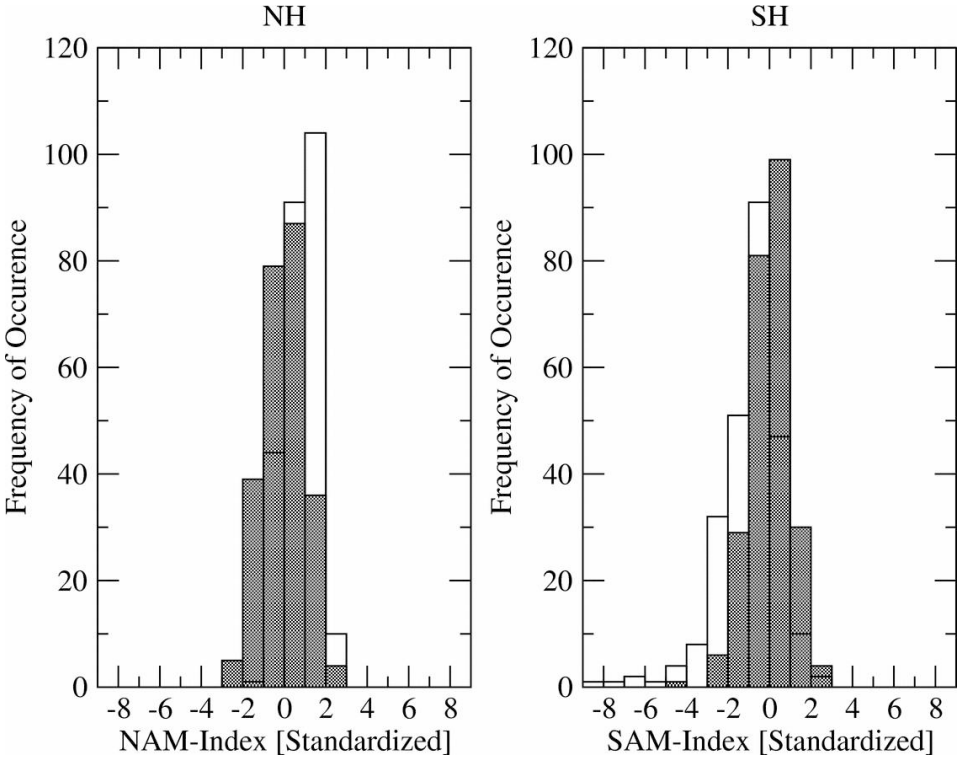

Fig. 5 Frequency of occurrence of the NAM (a) and SAM (b) index for the first (shaded bars) and second (white bars) five- year periods in the CCM3 experiments. Results are shown for DJF months.

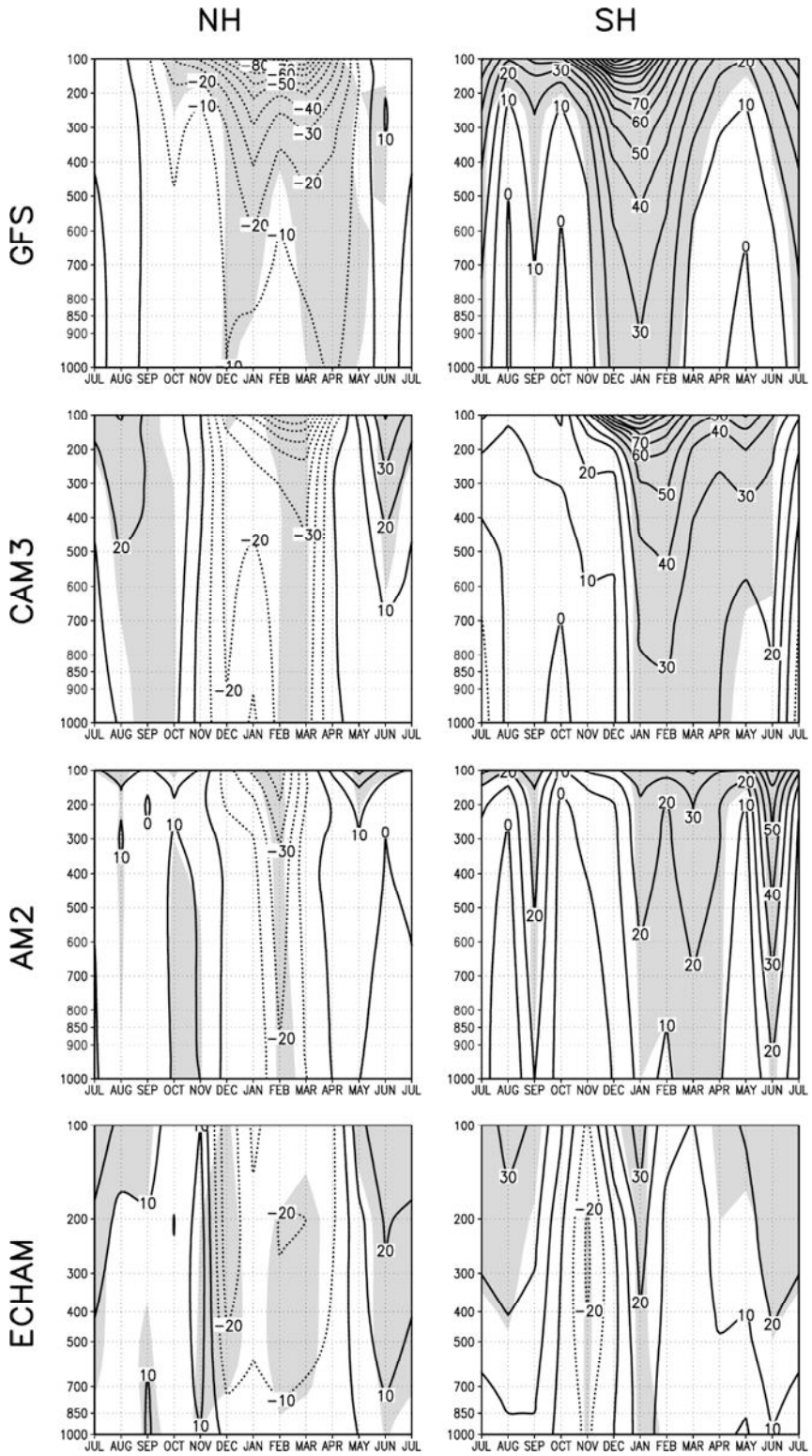

Fig. 6 As Fig. 3d and e, but the response in the GFS, the CAM3, the AM2, and the ECHAM5 experiments.

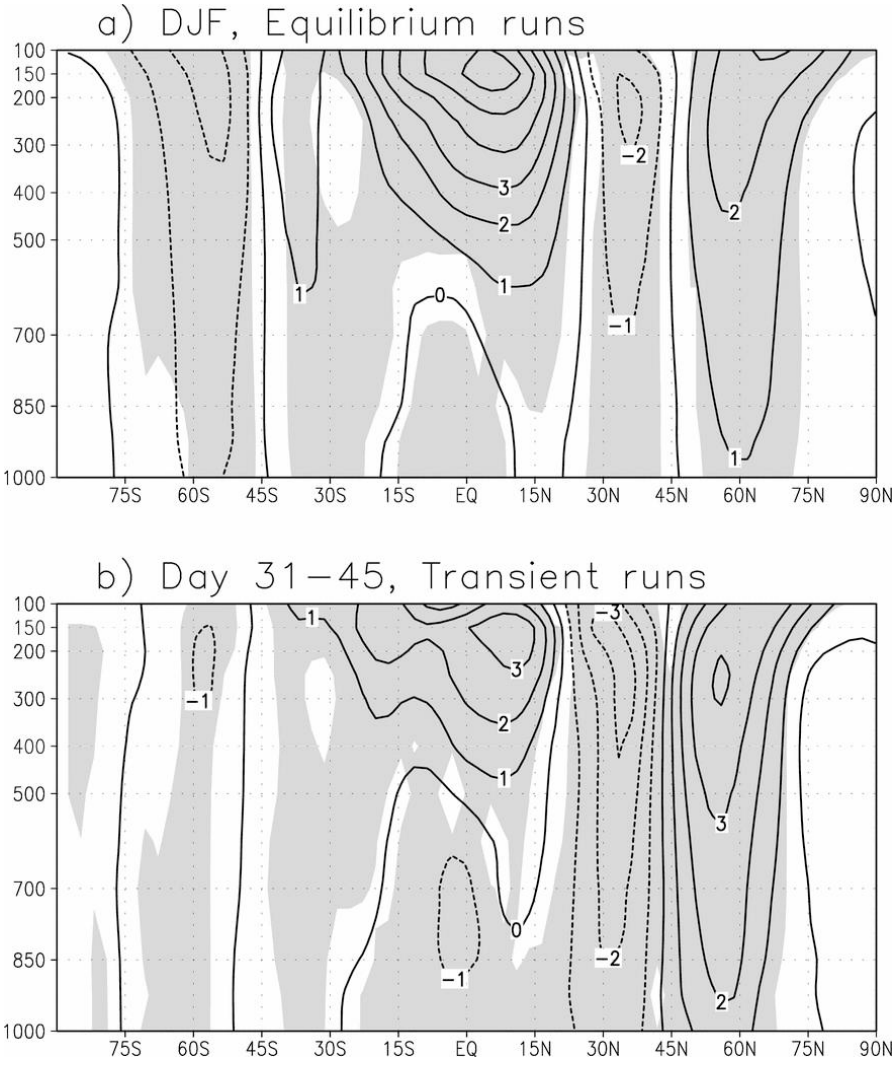

Fig. 7 DJF zonal-mean zonal wind response in the CCM3 experiments (upper panel) and the averaged response through day 31-45 in the CCM3 transient runs (lower panels). Unit: m s^{-1}. Shading in (a) indicates significant at the level of 95%.

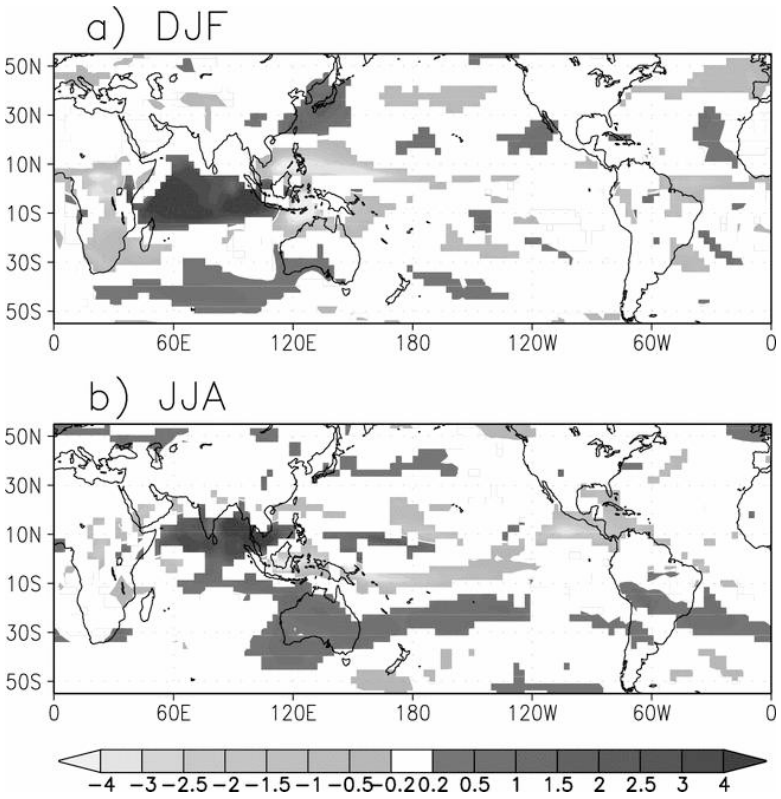

Fig. 8 Precipitation response in the CCM3 experiments. a) DJF, b) JJA. Displayed is just the response significant above 95%. Unit: mm day^{-1}.

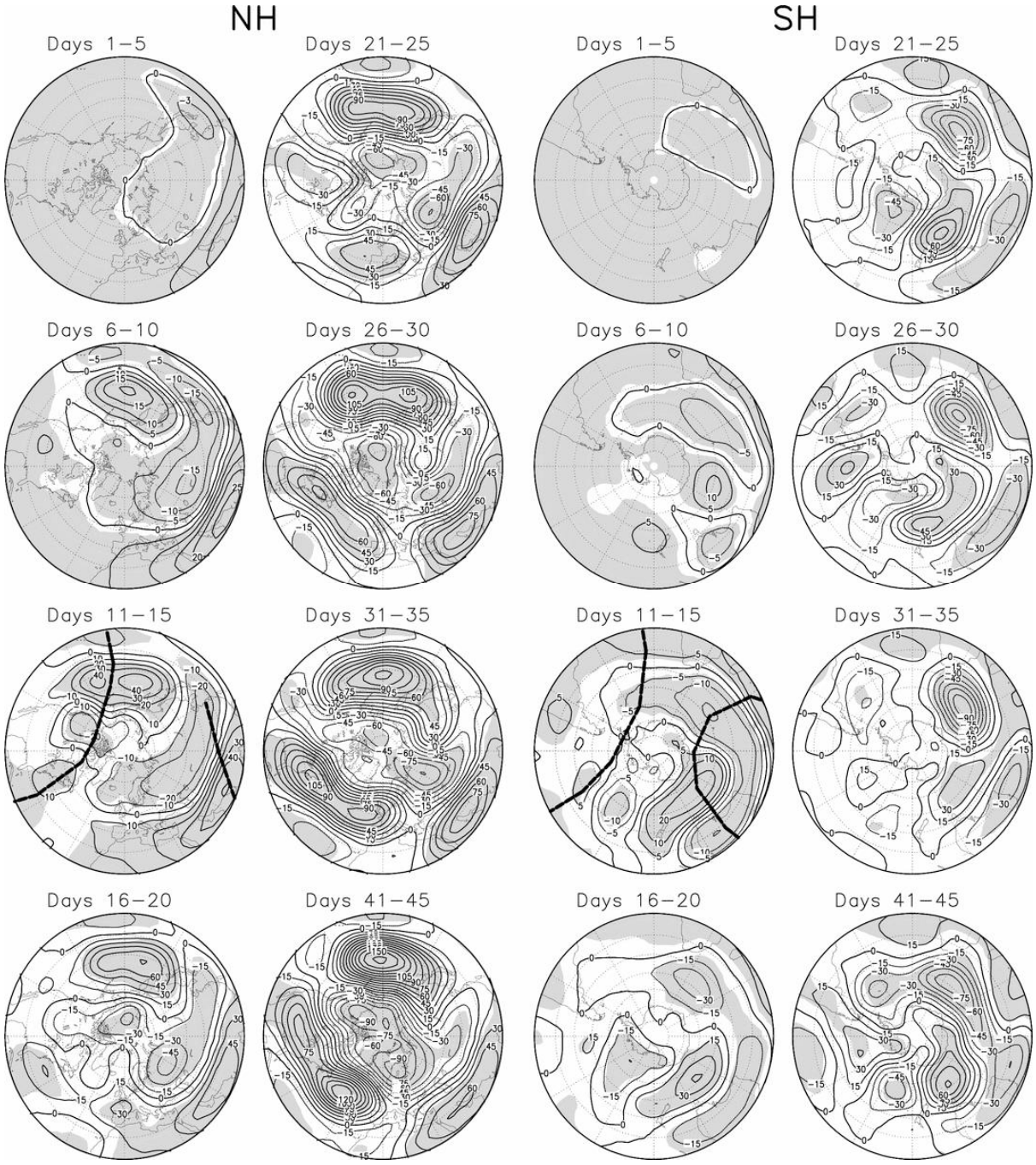

Fig. 9 The evolution of 200-hPa height responses in the CCM3 transient runs. Shading indicates significant at the level of 95%. Unit: gpm. The thick solid lines indicate propagation of wave trains.

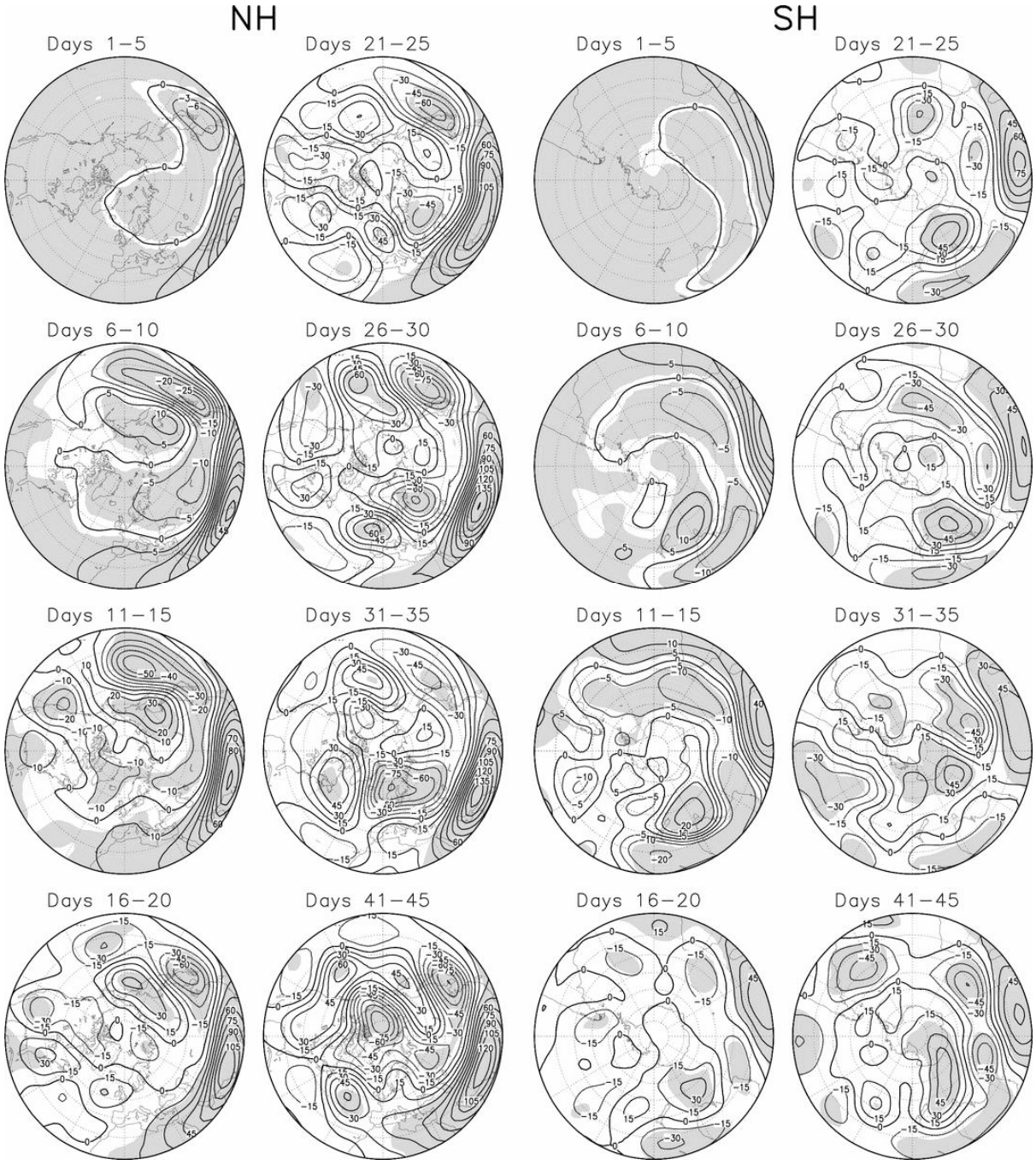

Fig. 10 As Fig. 9, but for the GFS experiments.

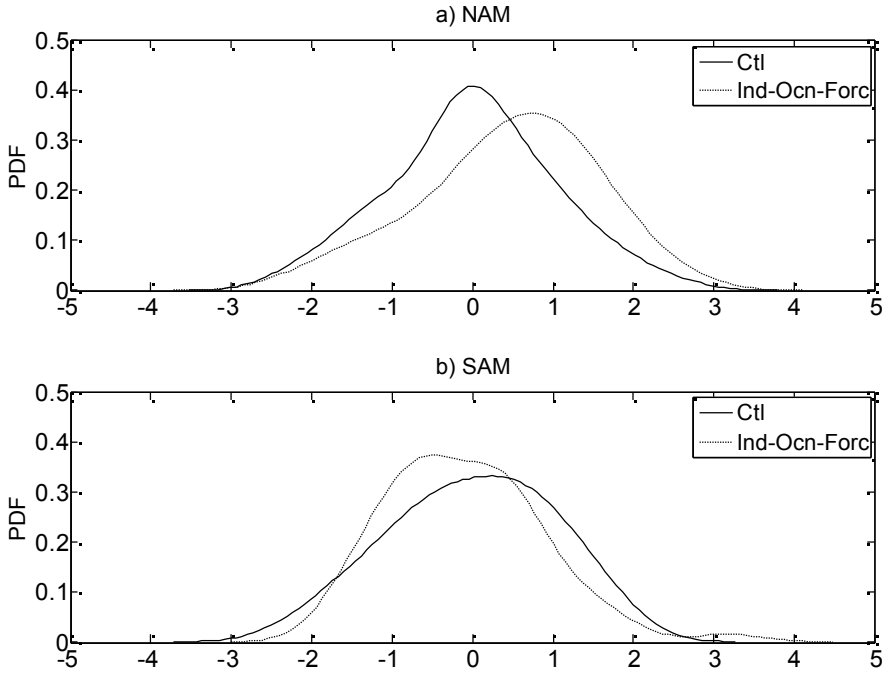

Fig. 11 Estimated Probability Distribution Functions (PDFs) of the normalized 200 hPa (a) NAM and (b) SAM indices determined from 41 to 45 day mean response in the CCM3 transient runs. The solid line is for control ensemble, and the dashed line is for the Indian Ocean forced ensemble.

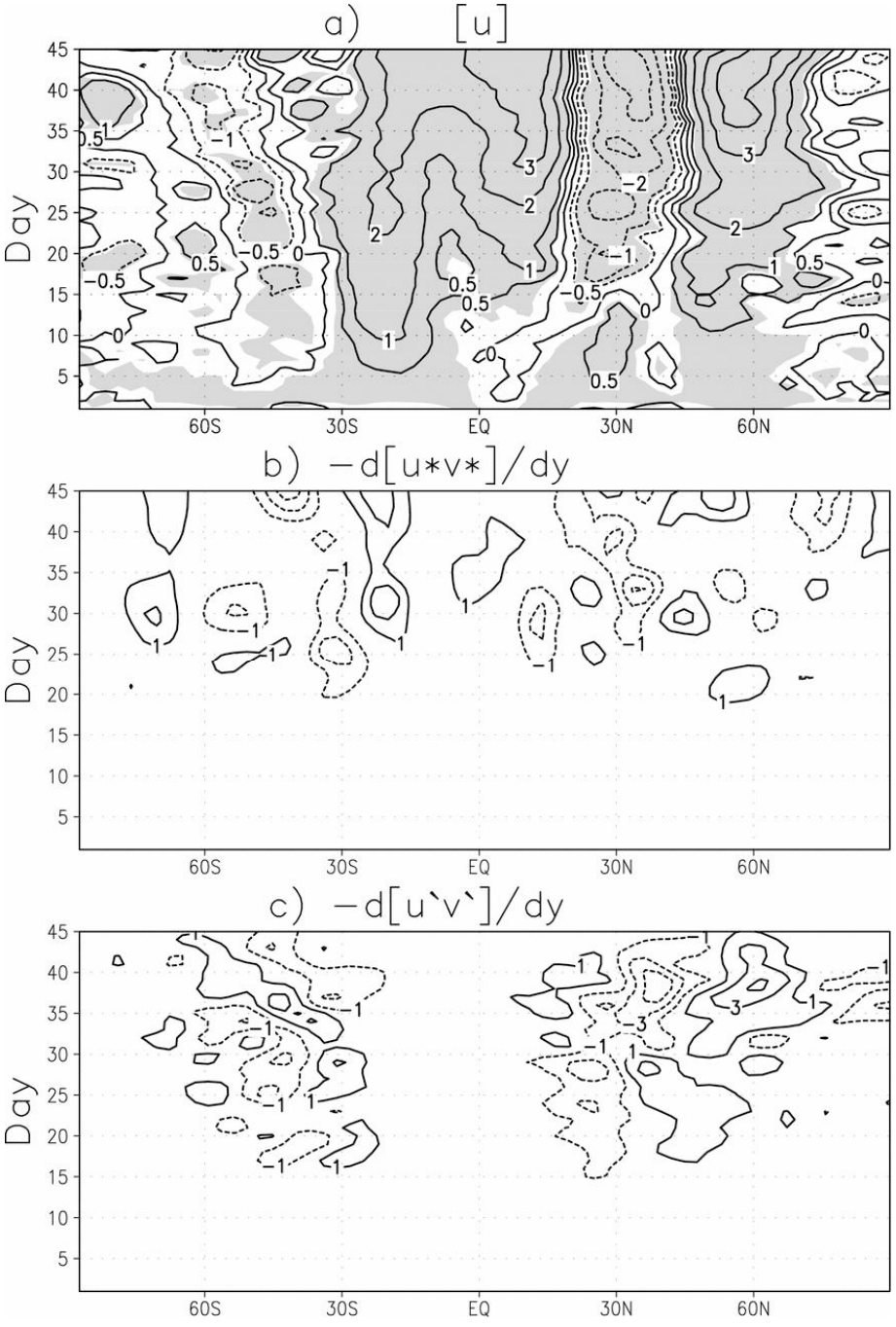

Fig. 12 The evolution of (a) the 300-hPa zonal-means zonal wind [u], (b) anomalous stationary wave momentum flux convergence ($-d\,[u^*v^*]/dy$), and (c) anomalous transient eddy momentum flux convergence ($-d[u'v']/dy$). Shading in (a) indicates statistical significance at the 95% level. Unit: ms^{-1} in (a), and ms^{-2} in (b, c).

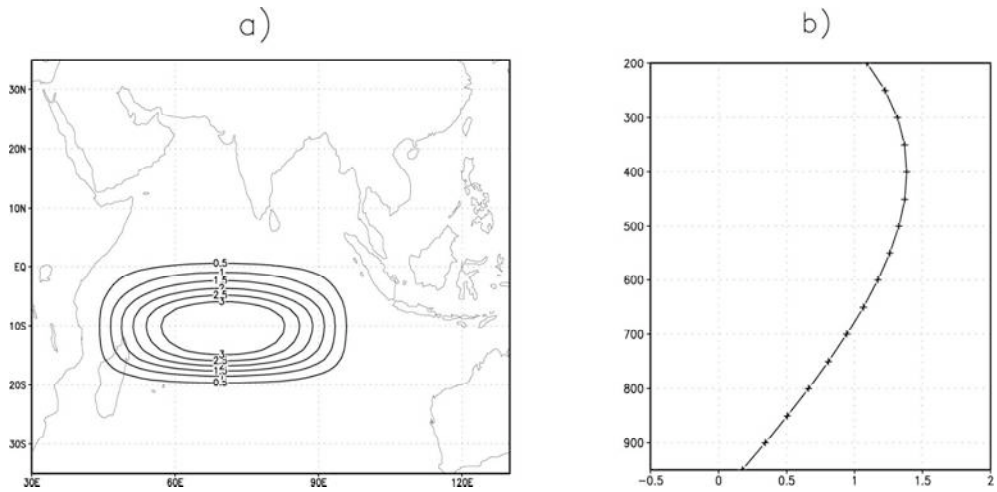

Fig. 13 The in-depth mean (a) and the vertical profile of the maximum center (b) of an idealized diabatic heating centering at (70^{o}E, 10^{o}S). Unit: K day^{-1}.

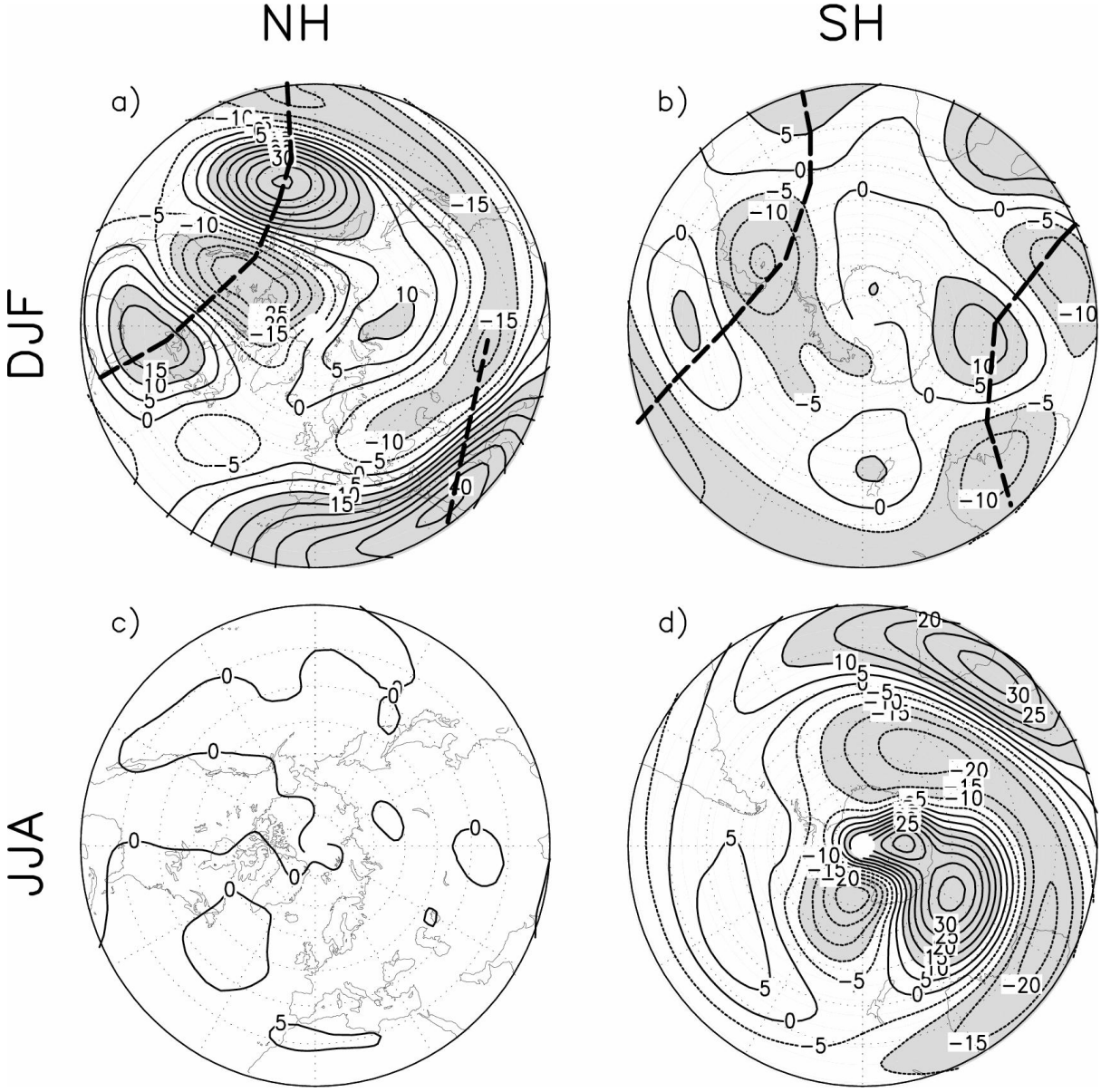

Fig. 14 LBM 200-hPa geopotential height responses to the idealized diabatic heating displayed in Fig. 13. (a, b) for the NH and the SH under the winter (DJF) basic state with the maximum heating at (70°E, 10°S), (c, d) as (a, b), but for the summer (JJA) basic state with the maximum heating at (90°E, 10°N). Unit: gpm. Shading indicates values greater than 10 gpm or less than –10 gpm in (a, d), and greater than 5 gpm or less than –5 gpm in (b, c). The thick solid lines indicate propagation of wave trains.